

# Cooperative Trajectory Planning for Haptic Shared Control between Driver and Automation in Highway Driving

Amir Benloucif, Anh-Tu Nguyen\*, *Member, IEEE*, Chouki Sentouh, *Member, IEEE*, Jean-Christophe Popieul

**Abstract**—This paper addresses the driver-automation shared driving control for lane keeping and obstacle avoidance of automated vehicles in highway traffic. The proposed shared control framework is established from a novel cooperative trajectory planning algorithm and a fuzzy steering controller. Based on polynomial functions, the cooperative trajectory planning is formulated by judiciously exploiting the information on the maneuver decision, the conflict management and the driver monitoring. As a result, the planned trajectory of the vehicle is *continuously* adapted according to the driver's actions and intentions. By means of Lyapunov stability arguments, sufficient conditions in terms of linear matrix inequalities are given to design a Takagi-Sugeno fuzzy model-based controller. This robust steering controller provides a necessary assistive torque to track the vehicle planned trajectory. The new shared driving control framework allows reducing effectively the driver-automation conflict issue while offering the driver more freedom to swerve within a predefined lane. The advantages of the proposed approach are evaluated using both objective and subjective results, experimentally obtained from several human drivers and an advanced interactive dynamic driving simulator.

**Index Terms**—Human-machine cooperation, vehicle control, haptic shared control, autonomous vehicles, cooperative trajectory planning, fuzzy control.

## I. INTRODUCTION

Recent technological breakthroughs in actuation, perception and artificial intelligence lead to a new dawn of driving assistance and highly automated driving. However, up to now the automation still remains imperfect and is prone to errors in the presence of human in the loop [1]. Haptic shared driving control has been shown as an effective scheme which allows to better meet the design guidelines of automation [2]–[5]. Keeping the human driver in the loop, these control schemes offer a *continuous* human-machine interaction since both the driver and the assistance driving system *simultaneously* control the vehicle through the steering wheel. This special feature of haptic shared control leads to many major advantages not only on the driver's workload and performance but also on the conflict management [1]. For the latter, since the driver *continually* has a haptic feedback from the automation, he/she is always able to counter the automation's actions in critical situations where the human-machine conflict cannot be avoided/solved.

Haptic shared driving control is described as a continuous spectrum extending from manual control to fully automated driving. Hence, the management of control authority between the driver and the automation is crucial for its successful applications. Moreover, the need for assistance and the performance of drivers strongly depend on the driving situation

[6]. Despite these facts, haptic shared control approaches that allow to *dynamically* manage the control authority between the driver and the assistance system have only appeared very recently, see for instance [6], [7]. In these works, the high-level information such as driver's state, environment perception, etc., is exploited to represent the driver's control authority. This information is then taken into account in the design of shared steering controllers which are able to provide appropriate assistive actions according to the driver's driving activities.

## A. Proposed Methodology

This paper proposes an alternative approach for haptic shared driving control in highway traffic. The proposed shared control architecture is composed of two hierarchical levels. The tactical level is responsible for driving decision making. The operational level aims to provide appropriate assistive actions to track the planned vehicle trajectory. A particular feature of the proposed shared control approach is that the driver-automation conflict is directly managed by a novel cooperative trajectory planner. This latter allows for a *continuous* adaptation of the vehicle trajectory according to the driving conditions. To this end, the tactical-level variables representing the control authority and the driving activities of human drivers are *explicitly* incorporated to construct the planning algorithm. As a result, the automation can plan the vehicle trajectories that better match the driver's intention to solve the conflict issue. A robust steering controller is designed at the operational level to provide a necessary assistive torque for trajectory tracking. The control design is based on the direct Lyapunov method and Takagi-Sugeno (T-S) fuzzy model-based technique [8]. As a result, sufficient design conditions are derived in terms of linear matrix inequalities (LMIs) which can be effectively solved with numerical solvers.

## B. Related Works on Vehicle Trajectory Planning

As the core element in automated driving, trajectory planning has been intensively investigated [9]. Numerous trajectory planning techniques with different degrees of computational complexity have been proposed [10]. Here, we adopt the so-called *hierarchical* planning approach [11], [12] to construct our cooperative trajectory planner. This is due to two main reasons. First, this approach is effective in terms of computational complexity and simple for real-time implementation [13]. Second, it provides a high-level interaction with drivers by communicating a finite set of feasible maneuvers [14], which corresponds to our need of a two-level (tactical and operational) cooperation between the driver and the automation for shared control.

Hierarchical planning is composed of a tactical-level maneuver planner and an operational-level trajectory generation algorithm. The former is in charge of *maneuver decision* to determine an appropriate maneuver among a finite set of maneuvers (lane changing, lane keeping, vehicle following, etc.) in a dynamic driving environment [14]. The operational planning algorithm aims at finding a solution for the selected maneuver while taking into account the vehicle dynamics. To

Manuscript received Month xx, 2xxx; revised Month xx, xxxx; accepted Month x, xxxx. This work was supported in part by the CoCoVeA project (Grant ANR-16-CE22-0007) through the Agence Nationale de la Recherche, in part by the ELSAT2020 project. \*Corresponding author: Anh-Tu Nguyen (e-mail: [nguyen.trananhthu@gmail.com](mailto:nguyen.trananhthu@gmail.com)).

The authors are with the laboratory LAMIH UMR CNRS 8201, Université Polytechnique Hauts-de-France, F-59313 Valenciennes, France.

this end, numerous existing planning techniques can be applied to generate a feasible trajectory for the vehicle [10]. Potential field approaches [15] have been intensively studied. Based on a discretization of the driving environment, these approaches can be formalized as a graph-search problem, especially with the well-known algorithms such as A\* search and its variants [16], [17]. The trajectory planning is formulated in [18]–[20] as a mathematical optimization problem. Interpolation-based approaches have also been widely applied to the geometric computation of trajectories. Several geometric forms have been used, including straight lines and arcs [21], clothoids [22], [23], etc. However, polynomial trajectories remain the most used forms in automated driving [14], [24], [25].

The proposed planning algorithm is inspired by the works presented in [14] and [25]. These latter are based on an exploration of polynomial trajectories which are subsequently evaluated via cost functions. Our algorithm combines the aspect of trajectory discretization from graph-search-based approaches with the cost evaluation from optimization-based ones to provide a flexible and efficient planning framework. It should be stressed that an important requirement of our cooperative planning algorithm is the high frequency of replanning. Indeed, it is crucial to take into account the fast variations of the driver's actions to avoid a long response time of the planned trajectories. This allows to avoid confusions which may lead to driver-automation conflict situations. For this reason, computation-intensive planning algorithms derived from, for instance, optimization-based approaches are not appropriate for our shared control purpose.

### C. Contributions

The proposed shared driving control approach leads to major advantages compared to existing works. Differently from [5]–[7] and numerous related references, the new approach offers the driver a freedom to choose a desired position within the road-lane, which is not always necessarily the lane centerline, so that he/she can swerve within the lane following his/her intention. As a consequence, the driver's driving effort and the driver-automation conflict can be effectively reduced. This obviously improves the *acceptability* of the proposed assistance driving system. Both objective and subjective results were experimentally performed with several human drivers and a dynamic driving simulator to demonstrate the effectiveness of the proposed method. To the best of our knowledge, the results on trajectory-planning-based shared driving control between human drivers and automation with experimental validations were not observed in any previous work.

The paper is organized as follows. Section II introduces the proposed architecture for haptic shared driving control. In Section III, we provide the details on the new cooperative trajectory planning algorithm. Section IV presents the design of a robust steering controller providing appropriate assistive actions for trajectory tracking control. The effectiveness of the new shared control approach is experimentally demonstrated in Section V with both objective and subjective results. Concluding remarks and future works are given in Section VI.

## II. HAPTIC SHARED DRIVING CONTROL ARCHITECTURE

This work focuses on highway driving with two main tasks: lane keeping and lane changing. The proposed architecture for haptic shared driving control using a cooperative trajectory planning is depicted in Fig. 1. This control architecture is composed of a tactical level and an operational level. The tactical level is in charge of the *driving decision making* which is concerned with the maneuver decision, the driver's intent inference, and the control authority management. It aims at determining the most appropriate maneuver to deal with a given driving situation. Especially, for highway driving, this level provides the choice of the reference lane, represented by

the lateral coordinate  $y_{target}$  of the desired lane-center, and the desired speed  $v_{target}$ . The decision making is based on an analysis of the data collected online from the driver, the vehicle and the driving environment. The details on the tactical level is out of the scope of this paper. The maneuver decision making, also called behavioral planning, is discussed in [14], [18], [26], whereas the tactical driver's behavior prediction and intent inference are well documented in [27], [28]. Here, the focus is on the haptic shared steering control between human drivers and the driving assistance system at the operational level. To this end, we only provide in the following the details on the two main components of this level, namely "Trajectory planning" and "Takagi-Sugeno fuzzy steering controller".

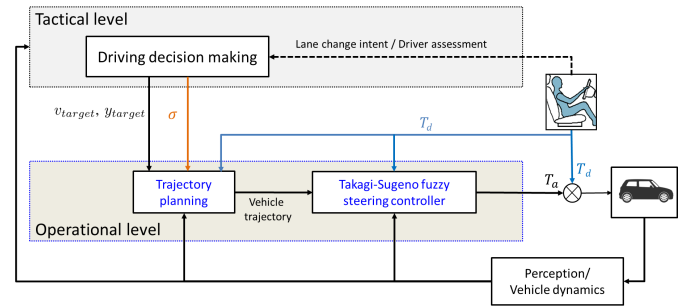


Fig. 1. Overview of the proposed haptic shared driving control structure.

The proposed cooperative trajectory planning algorithm is constructed as follows. The tactical level feeds the trajectory planner the position of the desired lane centerline  $y_{target}$  and the desired speed  $v_{target}$  to compute an appropriate vehicle trajectory. The driver's torque  $T_d$  applied on the steering wheel is also used for trajectory planning to adapt the planned trajectory according to the driver's actions. Moreover, the control authority management is crucial when the driver-automation conflicts occur. To this end, the authority variable  $\sigma$ , given by the tactical level, is incorporated in the trajectory planning to represent the driver's authority over the modification of the trajectory planned by the driving assistance system. This prevents involuntary or dangerous actions of drivers, especially in case of distraction and hypovigilance. As a result, the proposed trajectory planner generates appropriate trajectories to guide the vehicle within the lane (*i.e.*, lane keeping) or to execute lane-change maneuvers. Once the trajectory of the vehicle is planned, a robust steering controller is designed to compute a necessary assistive torque  $T_a$  for trajectory tracking purposes. This controller *simultaneously* acts on the steering wheel together with the human driver to achieve the driving goal since the human-machine conflict is considered upstream in the cooperative trajectory planning. Moreover, the physical limitations of the steering torque  $T_a$  is taken into account in the control design procedure. This offers the human driver a possibility to *override* the control actions issued from the automation in some emergency driving situations where the conflict issue cannot be solved/avoided. Further details on the tactical level are discussed below.

## III. COOPERATIVE TRAJECTORY PLANNING ALGORITHM

We describe step-by-step the proposed trajectory planning algorithm which is used for haptic shared driving control.

### A. Trajectory Planning Based on Polynomial Functions

Trajectory planning can be formulated as a boundary condition problem aiming to find a *smooth* trajectory that guides the vehicle from an initial state to a final one. The effectiveness of using polynomials for local trajectory planning in structured environments has been widely proved [14], [24]. It was shown in [29] that high-order polynomials (third-order or more) enable a simple planning formulation. Moreover, polynomial-based planning allows to compute *independently* lateral and longitudinal

vehicle motions while guaranteeing trajectories with *continuous* velocities, accelerations and curvatures [24].

For the lateral motion, the initial state  $[y_{r0} \ \dot{y}_{r0} \ \ddot{y}_{r0}]$  is composed of the current lateral position, speed and acceleration in the road reference frame. To define the final conditions of the vehicle lateral motion, it is assumed that the vehicle reaches the final target position  $y_{rf}$  with a zero lateral speed and acceleration. Hence, the final state of the lateral trajectory is given as  $[y_{rf} \ 0 \ 0 \ T_y]$ , where  $T_y$  is the lateral completion time. Thanks to six boundary conditions, it is possible to define a fifth-order polynomial representing the lateral motion to be performed as follows:

$$y_r(t) = \mathbf{b}_0 + \mathbf{b}_1 t + \mathbf{b}_2 t^2 + \mathbf{b}_3 t^3 + \mathbf{b}_4 t^4 + \mathbf{b}_5 t^5. \quad (1)$$

For the longitudinal motion, note that the final target position is unknown *a priori*. Hence, five boundary conditions allow to define a fourth-order polynomial representing the vehicle longitudinal motion from the initial state  $[x_{r0} \ \dot{x}_{r0} \ \ddot{x}_{r0}]$  to the final state  $[\dot{x}_{rf} \ 0 \ T_x]$ , where  $\dot{x}_{rf}$  is the final target speed and  $T_x$  is the longitudinal completion time:

$$x_r(t) = \mathbf{a}_0 + \mathbf{a}_1 t + \mathbf{a}_2 t^2 + \mathbf{a}_3 t^3 + \mathbf{a}_4 t^4. \quad (2)$$

From (1) and (2), the coefficients of both polynomials can be easily obtained by solving the following system of equations:

$$[\mathbf{a}_0 \ \mathbf{a}_1 \ \mathbf{a}_2 \ \mathbf{a}_3 \ \mathbf{a}_4]^\top = \mathcal{A} \mathcal{X}_r \quad (3)$$

$$[\mathbf{b}_0 \ \mathbf{b}_1 \ \mathbf{b}_2 \ \mathbf{b}_3 \ \mathbf{b}_4 \ \mathbf{b}_5]^\top = \mathcal{B} \mathcal{Y}_r \quad (4)$$

where the matrices  $\mathcal{A}$ ,  $\mathcal{B}$  depend on the completion times whereas the vectors  $\mathcal{X}_r$ ,  $\mathcal{Y}_r$  depend on the initial and the final target states as follows:

$$\mathcal{A} = \begin{bmatrix} 1 & 0 & 0 & 0 & 0 \\ 0 & 1 & 0 & 0 & 0 \\ 0 & 0 & 2 & 0 & 0 \\ 0 & 1 & 2T_x & 3T_x^2 & 4T_x^3 \\ 0 & 0 & 2 & 6T_x & 12T_x^2 \end{bmatrix}, \quad \mathcal{X}_r = \begin{bmatrix} x_{r0} \\ \dot{x}_{r0} \\ \ddot{x}_{r0} \\ \dot{x}_{rf} \\ \ddot{x}_{rf} \end{bmatrix},$$

$$\mathcal{B} = \begin{bmatrix} 1 & 0 & 0 & 0 & 0 & 0 \\ 0 & 1 & 0 & 0 & 0 & 0 \\ 0 & 0 & 2 & 0 & 0 & 0 \\ 1 & T_y & T_y & T_y^3 & T_y^4 & T_y^5 \\ 0 & 1 & 2T_y & 3T_y^2 & 4T_y^3 & 5T_y^4 \\ 0 & 0 & 2 & 6T_y & 12T_y^2 & 20T_y^3 \end{bmatrix}, \quad \mathcal{Y}_r = \begin{bmatrix} y_{r0} \\ \dot{y}_{r0} \\ \ddot{y}_{r0} \\ y_{rf} \\ \dot{y}_{rf} \\ \ddot{y}_{rf} \end{bmatrix}.$$

Remark from (3)-(4) that a polynomial trajectory can be completely defined when the initial state, the final target state and the completion time  $T_x$  and  $T_y$  are known. As shown below, manipulating these parameters of linear equations (3)-(4), a set of candidate trajectories can be generated. The planned trajectory to be performed by the ego-vehicle is selected among this trajectory set through an optimization-based evaluation while respecting the vehicle dynamics.

### B. Generation of Candidate Trajectories

At each replanning cycle  $T_{cycle}$ , a new set of trajectories must be generated. To guarantee the continuity of the vehicle trajectories, the generated trajectories share the same initial state. This latter is chosen from the trajectory computed in the previous cycle. Using the suffix  $\bullet_{prev}$  to refer to the trajectory computed in the previous cycle, the boundary conditions for the lateral and longitudinal motions are expressed as follows:

$$\begin{cases} y_{r0} = y_{r_{prev}}(T_{cycle}) \\ \dot{y}_{r0} = \dot{y}_{r_{prev}}(T_{cycle}) \\ \ddot{y}_{r0} = \ddot{y}_{r_{prev}}(T_{cycle}) \\ y_{rf} = y_{target} \\ \dot{y}_{rf} = 0 \\ \ddot{y}_{rf} = 0 \end{cases} \quad \text{and} \quad \begin{cases} x_{r0} = x_{r_{prev}}(T_{cycle}) \\ \dot{x}_{r0} = \dot{x}_{r_{prev}}(T_{cycle}) \\ \ddot{x}_{r0} = \ddot{x}_{r_{prev}}(T_{cycle}) \\ \dot{x}_{rf} = v_{target} \\ \ddot{x}_{rf} = 0 \end{cases}$$

Then, a set of lateral trajectories can be obtained by discretizing the final target position  $y_{target}$  and the completion time  $T_y$ .

In the same way, the discretization of the final target speed  $v_{target}$  and the completion time  $T_x$  allows generating a set of longitudinal trajectories. The discretizations are performed as

$$\dot{x}_{rf_i} = v_{target} + a_i \cdot \delta t, \quad a_i \in [-a_{lim}, a_{lim}] \quad (5)$$

$$y_{rf_j} = y_{target} + \Delta y_j, \quad \Delta y_j \in [-\Delta y_{lim}, \Delta y_{lim}] \quad (6)$$

$$T_{x_k} = k \cdot \Delta T, \quad T_{y_k} = k \cdot \Delta T, \quad k \in \{1, \dots, M\} \quad (7)$$

where  $a_i$  corresponds to an acceleration to be applied over a time interval  $\delta t$  to vary the final speed around  $v_{target}$ , and  $\Delta y_j$  is a deviation from the target lane centerline. The set of the final speeds is denoted by  $\dot{x}_{rf_i}$  in (5) whereas  $y_{rf_j}$  in (6) denotes the set of the final lateral positions. We distinguish between the tactical level in which the target lane centerline  $y_{target}$  is planned, and the lateral errors realized within the same lane that are associated with the operational level. Hence, the deviations  $\Delta y_j$  are limited to the interval  $[-\Delta y_{lim}, \Delta y_{lim}]$ , where  $\Delta y_{lim} \leq W/2$ , and  $W$  denotes the lane width.

The sets of the completion time of the longitudinal and lateral trajectories are respectively denoted as  $T_{x_k}$  and  $T_{y_k}$ , which are multiples of the time step  $\Delta T$ . Remark that  $M$  represents the maximum planning time, related to the maximum trajectory length. Then, the set of the longitudinal trajectories, denoted by  $x_{r_{ik}}$ , (respectively lateral trajectories, denoted by  $y_{r_{jk}}$ ) results from the combination of  $\dot{x}_{rf_i}$  with  $T_{x_k}$  (respectively  $y_{rf_j}$  with  $T_{y_k}$ ). Fig. 2 illustrates the process of generating trajectories in which Fig. 2 (a) shows a set of longitudinal speed profiles and Fig. 2 (b) provides an example of candidate trajectories to reach the lane centerline associated with  $y_{target} = 0$ .

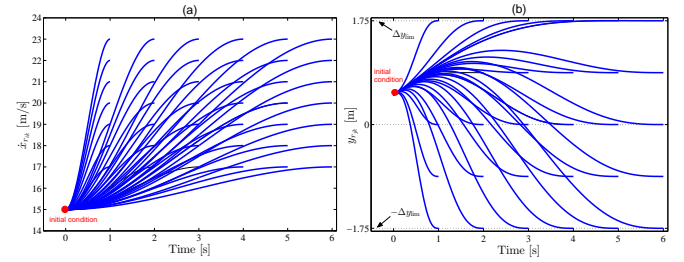


Fig. 2. Illustration of trajectories generation. (a) Set of speed profiles with  $\dot{x}_{r0} = 15$  [m/s] and  $v_{target} = 20$  [m/s]; (b) Set of trajectories to reach  $y_{target} = 0$  [m] from the initial state  $y_{r0} = 0.3$  [m] and  $\dot{y}_{r0} = 0.2$  [m/s].

In addition to the *continuity* of the planned trajectories, the choice of the initial state at each replanning cycle from the previously computed optimal trajectory is also to ensure the *temporal consistency* for each replanning cycle [25]. Indeed, if the condition of temporal consistency is not guaranteed, the planned trajectories can generate oscillations and overshoots. Therefore, the choice of the replanning cycle time  $T_{cycle}$  and the minimal completion time  $\Delta T$ , see (7), is crucial for trajectory planning performance. To guarantee the temporal consistency, the replanning cycle must be a multiple of the minimal completion time as follows:

$$T_{cycle} = N \cdot \Delta T, \quad N \leq M \quad (8)$$

where  $N$  is a positive integer and  $M$  is defined in (7). The relation (8) is justified by the uniqueness of the polynomial that links the initial state and the final state for a given completion time. Fig. 3 shows an example to illustrate the notion of temporal consistency. As depicted in Fig. 3 (a), at each replanning cycle, the newly generated trajectory is in continuity with that previously computed. This is not the case shown in Fig. 3 (b) for which the temporal consistency is not guaranteed due to an inappropriate choice of  $\Delta T$  and  $T_{cycle}$ .

### C. Real-Time Evaluation of Candidate Trajectories

Once the sets of candidate trajectories are generated, a real-time evaluation of these candidate trajectories is performed to

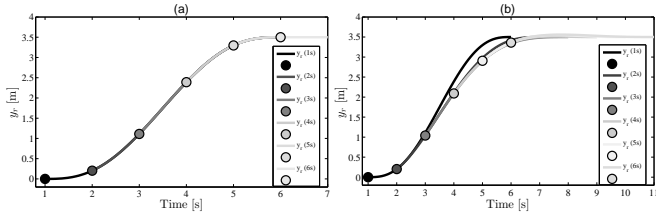


Fig. 3. Illustration of temporal consistency for trajectory planning. (a) Temporal consistency ensured with an appropriate choice of  $\Delta T$  and  $T_{cycle}$ ; (b) Temporal inconsistency due to an inappropriate choice of  $\Delta T$  and  $T_{cycle}$ .

choose those that will be executed by the ego-vehicle. Here, the evaluation process is performed according to a set of specifications on the driving comfort, the execution time of the maneuver, and the driver's desired position when he/she prefers to deviate from the planned trajectory. To this end, according to the expressions in (5), (6) and (7), we respectively define the cost functions related to the longitudinal and lateral motions as

$$\mathcal{C}_{x_{ik}} = w_{J_x} \mathcal{J}_{x_{ik}} + w_{T_x} T_{x_k} + w_v (\dot{x}_{rf_i} - v_{target})^2 \quad (9)$$

$$\mathcal{C}_{y_{jk}} = w_{J_y} \mathcal{J}_{y_{jk}} + w_{T_y} T_{y_k} + w_y (y_{rf_j} - y_{target})^2 + \mathcal{C}_{y_j} \quad (10)$$

with  $\mathcal{C}_{y_j} = \sigma w_d |y_{rf_j} - y_{des}|$ , where the desired position  $y_{des}$  of the driver and the control authority variable  $\sigma$  are specified later. The weighting coefficients  $w_{J_x}$ ,  $w_{J_y}$ ,  $w_{T_x}$ ,  $w_{T_y}$ ,  $w_v$ ,  $w_y$ ,  $w_d$ , are used to parameterize the type of the planned trajectories. The terms  $w_{J_x} \mathcal{J}_{x_{ik}}$  and  $w_{J_y} \mathcal{J}_{y_{jk}}$  allow to introduce the driving comfort in the trajectory evaluation process. These jerk-based terms are defined as

$$\mathcal{J}_{x_{ik}} = \int_0^{T_{x_k}} \ddot{x}_{r_{ik}}^2(\tau) d\tau, \quad \mathcal{J}_{y_{jk}} = \int_0^{T_{y_k}} \ddot{y}_{r_{jk}}^2(\tau) d\tau. \quad (11)$$

It is important to stress that due to the polynomial trajectory formulation as in (1) and (2), the jerk-related terms in (11) can be *analytically* expressed in function of the coefficients of the corresponding trajectories and the completion time as

$$\begin{aligned} \mathcal{J}_{x_{ik}} &= 12T_{x_k} (3a_{3_{ik}}^2 + 12a_{3_{ik}} a_{4_{ik}} T_{x_k} + 16a_{4_{ik}}^2 T_{x_k}^2), \\ \mathcal{J}_{y_{jk}} &= 12T_{y_k} (3b_{3_{jk}}^2 + 12b_{3_{jk}} b_{4_{jk}} T_{y_k} + 16b_{4_{jk}}^2 T_{y_k}^2 + \Xi_{jk}), \\ \Xi_{jk} &= 20b_{3_{jk}} b_{5_{jk}} T_{y_k}^2 + 60b_{5_{jk}} T_{y_k}^3 (b_{4_{jk}} + b_{5_{jk}} T_{y_k}). \end{aligned}$$

It should be highlighted that the above analytical expressions allow avoiding an intensive sampling procedure of the trajectories for evaluation purposes. This drastically reduces the computational burden to improve the effectiveness of the planning algorithm for practical use [10]. Note also that  $w_{T_x} T_{x_k}$  and  $w_{T_y} T_{y_k}$  are introduced into the cost functions to penalize the trajectories whose completion time is too large. In addition, the term  $w_v (\dot{x}_{rf_i} - v_{target})^2$  (respectively  $w_y (y_{rf_j} - y_{target})^2$ ) penalizes the trajectories whose final speed  $\dot{x}_{rf}$  (respectively final lateral position  $y_{rf}$ ) deviates from the target speed  $v_{target}$  (respectively target position  $y_{target}$ ). Finally,  $\sigma w_d |y_{rf_j} - y_{des}|$  is introduced to offer the driver a degree of freedom to deviate from the target lane centerline  $y_{target}$ . Weighted according to the driver-automation control authority variable  $\sigma$ , this term is particularly important to manage the conflict situations, in which the target position  $y_{target}$  and the driver's desired position  $y_{des}$  are inherently different. Hence, the driving goals of the driver and the assistance system are also different. This is the situation, for instance, when drivers must avoid undetected obstacles described in Section V-A.

The control authority variable  $\sigma \in [0, 1]$ , is provided by the driving decision making in the tactical level, see Fig. 1. This variable characterizes the control authority of the driver to modify the vehicle trajectory. In this work,  $\sigma$  is constructed such that the desired lateral position of the driver is ignored when

his/her torque is negligible or when he/she is out of his/her driving capacity. Hence,  $\sigma$  is proposed in the form

$$\sigma = DS \left( 1 - e^{-\varepsilon |T_d|} \right) \quad (12)$$

where  $\varepsilon$  is a scaling factor. The driver's state variable  $DS \in [0, 1]$  is introduced in (12) to take into account the driver's distraction in the trajectory planning. Note that  $DS = 1$  if the driver is not distracted and 0 otherwise. This continuous variable is provided by a driver monitoring system as in [7].

To determine the driver's desired position  $y_{des}$ , we propose to predict the lateral deviation that he/she desires to realize. Note that it is hard to perform such a deviation prediction basing only on the steering angle as in [15] since the measured steering angle is deduced from the summation of the driver's and the automations's torques. To overcome this, we predict the trajectory that the vehicle would have achieved with only the measured driver's torque  $T_d$ . Fig. 4 provides a detailed view of the "Trajectory planning" module shown in Fig. 1 and illustrates our approach to determine  $y_{des}$ . For a given  $T_d$ , the corresponding yaw rate  $r_d$  and yaw angle  $\psi_d$  can be determined using the well-known vehicle model (17). Together with the vehicle speed  $v_x$  and the road heading angle  $\psi_{road}$ ,  $r_d$  and  $\psi_d$  are input to a vehicle kinematic model to predict the lateral position over a time horizon, see Fig. 4. Here, we make use of the so-called *constant turn rate and velocity* (CTRV) model, depicted in Fig. 5, which has been widely exploited for prediction and tracking applications [30], [31].

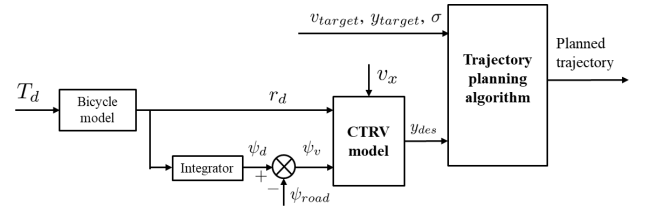


Fig. 4. Detailed view of the "Trajectory planning" module in Fig. 1.

The kinematic dynamics of the CTRV vehicle model is given as follows [30]:

$$\xi(t + \tau_p) = \begin{cases} x_g(t) + \mu(t) [\sin(\psi_v(t) + \tau_p r_d(t)) - \sin(\psi_v(t))] \\ y_g(t) + \mu(t) [\cos(\psi_v(t)) - \cos(\psi_v(t) + \tau_p r_d(t))] \\ \psi_v(t) + \tau_p r_d(t) \\ v_x(t) \\ r_d(t) \end{cases}$$

where  $\xi = [x_g \ y_g \ \psi_v \ v_x \ r_d]^T$  is the state vector,  $x_g$  and  $y_g$  are the coordinates of the vehicle gravity center,  $\psi_v = \psi_d - \psi_{road}$  is the vehicle yaw angle, and  $\mu = v_x / r_d$ . From the predicted lateral displacement  $\Delta y_{des}(\tau_p)$ , see Fig. 5, the desired lateral position of the driver is given by

$$y_{des} = y_g + \Delta y_{des}(\tau_p). \quad (13)$$

**Remark 1.** The value of  $\tau_p$  is crucial to obtain an effective trajectory planning algorithm. If the prediction horizon is too small, then the predicted trajectory is too close to the current trajectory which would not be useful to adapt the planned trajectory. However, a too large horizon leads to overshoots for the predicted trajectory and may cause instability in planned trajectories since the planning algorithm becomes too sensitive to the driver's torque. In our case, the choice of  $\tau_p = 1s$  was done experimentally to obtain a good steering comfort.

Once a candidate trajectory is generated, its heading angle  $\psi_r^*$  with respect to the global frame is determined as

$$\psi_r^* = \psi_r + \psi_{road}, \quad \psi_r = \arctan \left( \frac{\dot{y}_r}{\dot{x}_r} \right),$$



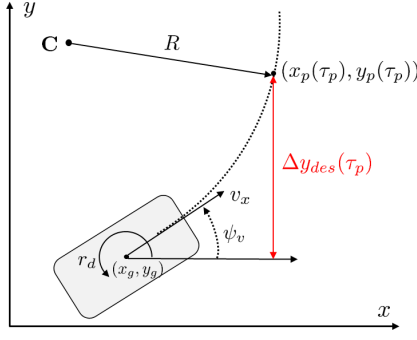


Fig. 5. Lateral displacement prediction over a time horizon  $\tau_p$ .

where  $\psi_r$  is the angle between the tangent of the candidate trajectory and that of the lane centerline,  $y_r$  and  $x_r$  are respectively given in (1) and (2). Note that the heading angle is back-transformed to global frame since the adherence to most vehicle dynamics constraints can only be verified there. Then, the trajectory curvature can be defined as follows [25]:

$$\kappa_r = \frac{d\psi_r}{ds_x} \quad (14)$$

where  $s_x$  is the covered arc length of the trajectory. The details on the determination of the trajectory curvature in the global frame can be found in [25]. To take into account the vehicle dynamics in the planning algorithm, the curvature  $\kappa_r$  defined in (14) should verify the following conditions:

$$|\kappa_r(t)| < |\kappa_{\max}^{\text{turn}}|, \quad |\kappa_r(t)| < |\kappa_{\max}^{\text{accel}}|, \quad \forall t \geq 0. \quad (15)$$

The admissible curvature to respect the minimal Ackerman's steering radius is defined as follows [32]:

$$\kappa_{\max}^{\text{turn}} = \frac{1}{\sqrt{l_r^2 + l^2 \cot^2(\delta_{\max})}},$$

where  $l_r$  is the distance of the rear tire from the gravity center,  $l$  is the vehicle wheelbase, and  $\delta_{\max}$  is the maximal steering angle at the wheels. The curvature limit to guarantee a given maximal lateral acceleration is expressed by

$$\kappa_{\max}^{\text{accel}} = \frac{a_{l \max}}{v_x^2},$$

where  $a_{l \max}$  is the maximal lateral acceleration to achieve a satisfactory driving comfort.

The trajectory evaluation process is characterized by the combination of the best longitudinal and lateral candidate trajectories. To this end, we define the global cost function for each combination as follows:

$$\mathbb{C}_{ijk} = \mathbb{C}_{x_{ik}} + \mathbb{C}_{y_{jk}} \quad (16)$$

where  $\mathbb{C}_{x_{ik}}$  and  $\mathbb{C}_{y_{jk}}$  are respectively given in (9) and (10). Minimizing the cost function  $\mathbb{C}_{ijk}$  defined in (16) while respecting the vehicle dynamics constraints (15), the trajectory executed by the ego-vehicle can be then determined.

#### D. Illustrative Results of Cooperative Trajectory Planning

Two experiments are performed to illustrate the results of the proposed cooperative trajectory planning algorithm. The objective is to show that in normal driving conditions, the vehicle trajectory can be *adaptively* planned following the driver's intention. Moreover, in some particular situations, the planning algorithm is able to guarantee a good tradeoff in terms of respecting aggressive driving behaviors and the vehicle dynamics to improve the comfort of passengers. The parameters of the cooperative planning algorithm are given in Table I.

TABLE I  
PARAMETERS OF THE COOPERATIVE PLANNING ALGORITHM.

$a_{l \lim} = 2 \text{ [m/s}^2\text{]}$	$\delta t = 3 \text{ [s]}$	$\Delta y_{\lim} = 1.75 \text{ [m]}$
$a_{l \max} = 3 \text{ [m/s}^2\text{]}$	$\Delta T = 0.1 \text{ [s]}$	$T_{\text{cycle}} = 0.1 \text{ [s]}$
$\delta_{\max} = 55 \text{ [deg]}$	$w_{J_x} = 3 \text{ [-]}$	$w_{J_y} = 0.05 \text{ [-]}$
$w_{T_x} = 3 \text{ [-]}$	$w_{T_y} = 3 \text{ [-]}$	$w_v = 1.5 \text{ [-]}$
$w_y = 2 \text{ [-]}$	$w_d = 10 \text{ [-]}$	$M = 60 \text{ [-]}$

1) *Experiment 1 [Normal Steering Behavior]*: This test is composed of two phases, see Fig. 6. From 0s to 4s (Phase 1), the driver's torque is negligible. During Phase 2 (from 4s to 15s), we apply to the steering wheel a sinusoidal torque of an amplitude  $A_t = 3 \text{ [Nm]}$  and a period  $T_t = 8 \text{ [s]}$ . As observed in Fig. 6 (a)<sup>1</sup>, the planned trajectory corresponds to the lane centerline in Phase 1. During Phase 2, the planned trajectory is in the direction of the applied driver's torque to bring the vehicle to the driver's desired position  $y_{des}$  expressed in (13) by deviating it from the lane centerline. At 8s, the driver's torque becomes negative and the planned trajectory returns to the lane centerline. Remark that the planned trajectory is always within the lane limits  $[-1.75, 1.75]$ . Figs. 6 (b) and (d) show the corresponding planned lateral speed and acceleration. Observe that the trajectory acceleration amplitude is quite small (less than  $2 \text{ [m/s}^2\text{]}$ ) during the whole experiment), which can lead to a good driving comfort. Although there is a small lag between the measured torque  $T_d$  and other planned signals, inherently due to the vehicle dynamics and the planning computation, we can see that the planned trajectory *adaptively* follows the driver's intention during this experiment.

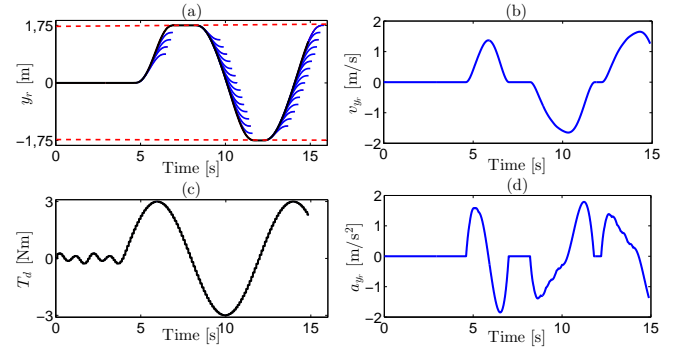


Fig. 6. Experiment 1. (a) Planned vehicle trajectory; (b) Driver torque; (c) Planned lateral speed; (d) Planned lateral acceleration.

2) *Experiment 2 [Aggressive Steering Behavior]*: This test is also composed of two similar phases, for which we consider a more aggressive steering behavior with a sinusoidal torque  $T_d$  of the same amplitude  $A_t = 3 \text{ [Nm]}$  and a period  $T_t = 4 \text{ [s]}$  during Phase 2, see Fig. 7 (b). We remark that to respect the vehicle dynamics constraints (15), the lag between the measured torque  $T_d$  and other planned signals is more important (more than  $0.5s$ ) compared to that of the previous experiment. As shown in Figs. 7 (a), (b) and (d), the planned trajectories are much faster than those in Experiment 1 to follow the high-frequency change of the driver's steering action. This leads to a higher amplitude of the planned lateral acceleration in this case, which is however still reasonable and less than the predefined value  $a_{l \max} = 3 \text{ [m/s}^2\text{]}$ . Moreover, due to the consideration of this maximal admissible lateral acceleration, the planned trajectory changes the direction even before reaching the lane boundaries since the driver's torque direction has already been changed, see Figs. 7 (a), (b). Hence, there is a tradeoff between the respect for the driver's actions and that of the vehicle dynamics for driving comfort reasons.

<sup>1</sup>The planned trajectories at each planning cycle are plotted in blue, and the concatenation of the executed trajectory is plotted in black.

From the above illustrative results, it can be seen that the proposed planning algorithm can adaptively generate the vehicle trajectory under different driver's steering behaviors while being able to guarantee a good driving comfort. The effectiveness of this algorithm in terms of solving the driver-automation conflict is further discussed in Section V.

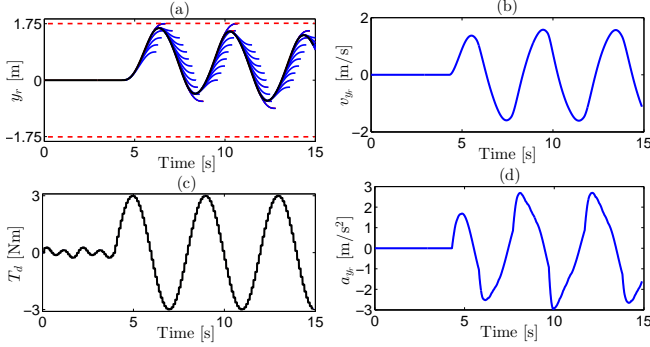


Fig. 7. Experiment 2. (a) Planned vehicle trajectory; (b) Driver torque; (c) Planned lateral speed; (d) Planned lateral acceleration.

#### IV. TAKAGI-SUGENO FUZZY MODEL-BASED CONTROL

After the trajectory is planned following the driver's intention, the ego-vehicle should track this trajectory. This section presents the design of a robust steering controller which produces necessary assistive torque for trajectory tracking.

##### A. Driver and Vehicle Modeling

Hereafter, we briefly review the driver-vehicle modeling for lateral control. The nomenclature is given in Table II.

TABLE II  
NOMENCLATURE.

Notation	Description
$v_x$	vehicle longitudinal speed [m/s]
$v_y$	vehicle lateral speed [m/s]
$\beta$	vehicle sideslip angle [rad]
$r$	vehicle yaw rate [rad/s]
$\psi_L$	relative yaw angle [rad]
$y_L$	lateral offset from the centerline [m]
$\delta_d$	steering wheel angle at the column system [rad]
$T_a$	assistive torque [Nm]
$T_d$	driver torque [Nm]

1) *Road-Vehicle Model with Steering Assistance System:* For shared steering control purposes, the following road-vehicle system integrating the electric power steering model is used [6]:

$$\dot{\mathbf{x}}_v = A_v \mathbf{x}_v + B_v(T_a + T_d) + E_v \mathbf{w} \quad (17)$$

where  $\mathbf{x}_v = [\beta \ r \ \psi_L \ y_L \ \delta_d \ \dot{\delta}_d]^\top$  is the vehicle state. The road curvature  $\mathbf{w}$  represents the planned trajectory. The state-space matrices of (17) are given by [6].

2) *Driver-in-the-Loop Vehicle Model:* To take into account the driver-automation interaction at the steering wheel, a human driver model is integrated into the road-vehicle system for shared control purposes. To this end, the following two-point visual model being able to reproduce the driver's *compensatory* and *anticipatory* behaviors is used [7]:

$$\dot{\mathbf{x}}_d = A_d \mathbf{x}_d + B_d \mathbf{u}_d, \quad \mathbf{u}_d = C \mathbf{x}_v, \quad \mathbf{y}_d = C_d \mathbf{x}_d \quad (18)$$

where  $\mathbf{x}_d = [\mathbf{x}_{d1} \ \mathbf{x}_{d2}]^\top$ . The state  $\mathbf{x}_{d1}$  represents the driver's perception of the steering wheel correction. The state  $\mathbf{x}_{d2}$  is the driver's torque which is also the output, i.e.,  $\mathbf{x}_{d2} = \mathbf{y}_d = T_d$ .

The state-space matrices of system (18) are detailed in [7]. From (17) and (18), the driver-vehicle model can be expressed as

$$\dot{\mathbf{x}} = \mathbf{A}(v_x) \mathbf{x} + \mathbf{B} T_a + \mathbf{E}(v_x) \mathbf{w} \quad (19)$$

where  $\mathbf{x} = [\mathbf{x}_v^\top \ \mathbf{x}_d^\top]^\top$  and

$$\mathbf{A}(v_x) = \begin{bmatrix} A_v & B_v C_d \\ B_d C & A_d \end{bmatrix}, \quad \mathbf{B} = \begin{bmatrix} B_v \\ 0 \end{bmatrix}, \quad \mathbf{E}(v_x) = \begin{bmatrix} E_v \\ 0 \end{bmatrix}.$$

Note that the notations  $\mathbf{A}(v_x)$  and  $\mathbf{E}(v_x)$  are to make clear that these matrices depend on the time-varying parameter  $v_x$ .

**Remark 2.** The driver-in-the-loop vehicle model (19) has been identified with the driving data of nine human driver participants, collected from the SHERPA simulator (see Section V) in real-world driving situations. More details on this control-based model (19) can be found in [7].

3) *Control Performance Specifications:* To improve the closed-loop control performance, the controlled output of system (19) can be defined as

$$\mathbf{z} = [a_y \ \mathbf{u}_d^\top \ \dot{\delta}_d]^\top. \quad (20)$$

The driving comfort is represented by the lateral acceleration  $a_y$  and the steering rate  $\dot{\delta}_d$ . The tracking performance and the driver's anticipatory behavior are represented through  $\mathbf{u}_d$ . Note also that all components of  $\mathbf{z}$  can be expressed by those of  $\mathbf{x}$  in (19) as  $\mathbf{z} = \mathbf{C}(v_x) \mathbf{x}$ , see the details in [7].

For digital control implementation, the Euler discretization method is used to derive the following discrete-time counterpart of the continuous-time system (19):

$$\Sigma(v_x) : \begin{cases} \mathbf{x}_{\kappa+1} = A(v_x) \mathbf{x}_\kappa + B T_a + E(v_x) \mathbf{w}_\kappa \\ \mathbf{z}_\kappa = C(v_x) \mathbf{x}_\kappa \end{cases} \quad (21)$$

where  $A(v_x) = I + T_e \mathbf{A}(v_x)$ ,  $B = T_e \mathbf{B}$ ,  $E(v_x) = T_e \mathbf{E}(v_x)$  and  $C(v_x) = \mathbf{C}(v_x)$ . The sampling time is  $T_e = 0.01$ s, and  $\mathbf{z}_\kappa$  denotes the value of the signal  $\mathbf{z}$  taken at the  $\kappa$ -instant.

4) *T-S Fuzzy Representation of Driver-Vehicle Model:* There are three time-varying parameters involved in the state-space matrices of system  $\Sigma(v_x)$  defined in (21), i.e.,  $\theta_* = [v_x \ \frac{1}{v_x} \ \frac{1}{v_x^2}]^\top$ . Hence, using the sector nonlinearity approach [8, Chapter 2], the corresponding T-S fuzzy representation of model (21) has  $2^3 = 8$  linear subsystems. This leads to conservative design results since the terms  $v_x$ ,  $\frac{1}{v_x}$  and  $\frac{1}{v_x^2}$  are considered *separately* though they are strongly dependent [6]. To reduce both the conservatism and the numerical complexity for the control design, the following variable change is used:

$$v_x = \frac{v_0 v_1}{v_1 + v_0 \theta} \Leftrightarrow \frac{1}{v_x} = \frac{1}{v_0} + \frac{1}{v_1} \theta \quad (22)$$

where  $\theta_{\min} \leq \theta \leq \theta_{\max}$ , with  $\theta_{\min} = -1$  and  $\theta_{\max} = 1$ . The two constants  $v_0$  and  $v_1$  are given by

$$v_0 = \frac{2v_{\min} v_{\max}}{v_{\min} + v_{\max}}, \quad v_1 = \frac{2v_{\min} v_{\max}}{v_{\min} - v_{\max}}.$$

Note that since  $v_x = v_{\min} = 8$  [m/s] for  $\theta = \theta_{\min}$  and  $v_x = v_{\max} = 30$  [m/s] for  $\theta = \theta_{\max}$ , the new premise variable  $\theta$  can be thus used to describe the variation of  $v_x$  between its lower and upper bounds. Moreover, applying the Taylor's approximation as in [6] to the second expression of (22) yields

$$v_x \simeq v_0 \left(1 - \frac{v_0}{v_1} \theta\right), \quad \frac{1}{v_x^2} \simeq \frac{1}{v_0^2} \left(1 + 2 \frac{v_0}{v_1} \theta\right). \quad (23)$$

Substituting these expressions into (21) leads to the driver-in-the-loop vehicle model  $\Sigma(\theta)$ , which is linearly dependent only

on  $\theta$ . Using the sector nonlinearity approach [8],  $\Sigma(\theta)$  can be exactly represented in the T-S fuzzy form

$$\Sigma(\theta) : \begin{cases} \mathbf{x}_{\kappa+1} = \sum_{i=1}^2 \eta_i(\theta) (A_i \mathbf{x}_{\kappa} + B \text{sat}(\mathbf{u}_{\kappa}) + E_i \mathbf{w}_{\kappa}) \\ \mathbf{z}_{\kappa} = \sum_{i=1}^2 \eta_i(\theta) C_i \mathbf{x}_{\kappa} \end{cases} \quad (24)$$

where  $T_a = \text{sat}(\mathbf{u}) = \text{sign}(\mathbf{u}) \min(|\mathbf{u}|, \bar{T}_a)$ . The steering control action  $\mathbf{u}$  is designed such that the vehicle follows the trajectory provided by the cooperative trajectory planning algorithm in Section III. The maximal value of the assistance steering torque is fixed as  $\bar{T}_a = 6$  [N/m] which is appropriate for highway driving conditions. The details of these submodels ( $A_i, E_i, C_i$ ) and the corresponding membership functions  $\eta_i(\theta)$ ,  $i = 1, 2$ , of the T-S fuzzy model (24) are easily obtained and thus omitted here for brevity.

**Remark 3.** The use of the variable change (22) together with the Taylor's approximation (23) allows to decrease the number of linear submodels of the vehicle T-S fuzzy model from eight to two, see (24). This leads to a great advantage in terms of reducing not only the design conservatism but also the numerical complexity for real-time implementation.

**Remark 4.** For highway driving, the amplitude of the road curvature  $\mathbf{w}$  is small and always satisfies

$$\mathbf{w} \in \mathcal{W}_{\rho} = \{\mathbf{w} : \mathbb{R}^+ \mapsto \mathbb{R}, \quad \mathbf{w}^T \mathbf{w} \leq \rho\} \quad (25)$$

for some scalar  $\rho > 0$ . In this study, we choose  $\rho = \frac{1}{R_{\min}^2}$  where  $R_{\min} = 50$  [m] is a reasonable minimal value of the curvature radius for highway driving.

### B. LMI-Based Takagi-Sugeno Fuzzy Control Design

The dynamics of the driver-vehicle system (24) depends on the *time-varying* parameter  $\theta$ . In addition, as mentioned above, the control input saturation should be *explicitly* considered in the control design to improve both the safety and the comfort of passengers. The following theorem provides an effective framework to handle these practical control issues. Note that for a matrix  $\mathcal{M}$ ,  $\mathcal{M} \succ 0$  (respectively  $\mathcal{M} \prec 0$ ) indicates that  $\mathcal{M}$  is symmetric positive (respectively negative) definite.

**Theorem 1.** Given a driver-vehicle model in the T-S fuzzy form (24) with  $\mathbf{w}$  satisfying (25), and a positive scalar  $\tau_1 < 1$ . If there exist symmetric matrices  $X_i \succ 0$ , diagonal matrices  $S_i \succ 0$ , matrices  $H, G_i, W_i$  of appropriate dimensions,  $i = 1, 2$ , and positive scalars  $\tau_2, \gamma$  such that

$$\begin{aligned} 1 - \tau_1 - \tau_2 \rho &> 0, \\ \begin{bmatrix} H + H^T - X_i & \star \\ G_i - W_i & \bar{T}_a^2 \end{bmatrix} &\succeq 0, \\ \begin{bmatrix} H + H^T - X_i & \star \\ C_i H & \gamma I \end{bmatrix} &\succeq 0, \\ \begin{bmatrix} \tau_1(X_i - H - H^T) & \star & \star & \star \\ W_i & -2S_i & \star & \star \\ 0 & 0 & -\tau_2 I & \star \\ A_i H + B G_i & -B S_i & E_i & -X_k \end{bmatrix} &\prec 0, \end{aligned}$$

for  $i, k = 1, 2$ . Then, the parameter-dependent control law

$$\mathbf{u}(\kappa) = \sum_{i=1}^2 \eta_i(\theta) K_i \mathbf{x}(\kappa), \quad \text{with } K_i = G_i H^{-1} \quad (26)$$

stabilizes the saturated system (24) while guaranteeing the  $\mathcal{L}_{\infty}$ -performance  $\mathbf{z}^T \mathbf{z} \leq \gamma$  with  $\mathbf{z}$  defined in (20).

*Proof.* The proof can be completed along the similar lines of reasoning as in [33, Theorem 2], and it is omitted here.  $\square$

**Remark 5.** The decay rate  $\tau_1$  plays an important role in the time performance of the closed-loop system [8]. Indeed, a large value of this tuning parameter yields a fast closed-loop convergence. However, the resulting controller may induce aggressive behaviors, especially in the presence of system disturbances. For this study, a value of  $\tau_1 = 0.1$  allows achieving a satisfactory path following performance.

**Remark 6.** The control design in Theorem 1 is a simplified version of that in [33, Theorem 2] since the input matrix  $B$  in (24) is *constant*. In particular, controller (26) does not require any matrix inversion of parameter-dependent feedback gain, which greatly simplify the real-time control implementation. Note that the design conditions in Theorem 1 are expressed in terms of LMIs. Hence, the feedback gains  $K_i$ ,  $i = 1, 2$ , in (26) can be easily computed with Matlab software [33].

## V. HARDWARE EXPERIMENTS WITH HUMAN DRIVERS

This section presents an evaluation study to verify the effectiveness of the proposed cooperative trajectory planning algorithm for driver-automation haptic shared driving.

### A. Experimental Setup

1) *Driving Simulator:* The evaluation study was performed with a SHERPA driving simulator. This simulator is based on a Peugeot 206 mock-up fixed on a Stewart platform, the overall is positioned in front of five flat panel displays providing a visual field of  $240^\circ$ , see Fig. 8. The simulator is equipped with an active steering wheel and sensors providing the measurements of steering angle, steering rate and steering torque. It is also equipped with a force feedback gas pedal and a driver monitoring system, both from Continental Automotive company. Using the SCANeR environment, all planning and control algorithms are implemented in the SHERPA simulator through Matlab/Simulink software.



Fig. 8. SHERPA driving simulator.

2) *Driver Participants:* Six participants took part in the evaluation experiment. The average age was  $32 \pm 10$  years old. All participants are experienced drivers and reported an average annual mileage of 15,000 km.

3) *Test Protocol:* To illustrate the interest of the proposed cooperative planning algorithm for haptic shared driving, a short scenario of obstacle avoidance is considered. The experiment takes place on a straight two-lane road of 4 km. With instructions to stay within the lane, drivers are required to avoid other vehicles stopped and placed so as to partially block the lane. Groups of four vehicles constitute an obstacle avoidance situation as shown in Fig. 9. Three types of situations distinguished by the spacing between the vehicles are respectively defined with a spacing of 150m, 100m and 50m. In total, six obstacle avoidance situations were randomly arranged on the test track. Here, we assume that the obstacles are *undetected* by the vision system and the driver participants must perform an obstacle avoidance maneuver to avoid the collisions at a constant speed  $v_x = 90$  [km/h]. With the same scenario, the participants tested the three following strategies.

- **Manual Control.** Only drivers performed the driving.



- **No-Shared Control.** The drivers performed the driving task with a conventional lane keeping system, *i.e.*, the only goal of this latter is to track the lane centerline.
- **Shared Control.** The drivers performed the driving with a lane keeping system integrating the proposed cooperative trajectory planning algorithm.

These strategies were tested in a *random* order. Before the test, each participant realized a short “familiarization” phase to perform a driving task on a free test track with these strategies.

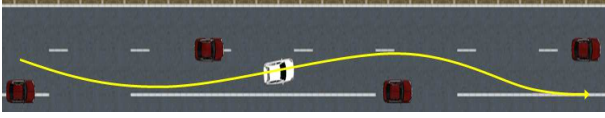


Fig. 9. Test scenario on collision avoidance with other vehicles stopped on both sides of the track.

#### 4) Evaluation Criteria:

a) *Objective Evaluation:* This evaluation is based on mathematical metrics to analyze the driver-automation interaction as well as the quality of the (shared) driving control. Four criteria are proposed to evaluate the driver-automation interaction: time consistency  $TiC$ , effort consistency  $EfC$ , steering effort  $StE$ , and steering resistance  $StR$ , see also [6]. The time consistency metric is defined as follows:

$$TiC = \frac{\mathcal{T}_c}{\mathcal{T}_{sc}}, \quad \text{with } \mathcal{T}_c = \{t \in [0, \mathcal{T}_{sc}] : T_d(t) \cdot T_a(t) > 0\},$$

where  $\mathcal{T}_{sc}$  is the scenario duration, and  $\mathcal{T}_c$  is the duration in which the automation *cooperatively* shares the vehicle control with the driver. The effort consistency metric is defined as

$$EfC = \frac{\int_{\mathcal{T}_c} T_a^2(\tau) d\tau}{\int_{\mathcal{T}_{sc}} T_a^2(\tau) d\tau}.$$

Note that these two metrics allow to evaluate the consistency between the driver and the automation. The total effort provided by the driver during the test scenario is defined as

$$StE = \int_{\mathcal{T}_{sc}} T_d^2(\tau) d\tau.$$

Finally, the total resisting effort delivered by the driving automation during the test scenario is given by

$$StR = \int_{\mathcal{T}_r} T_a^2(\tau) d\tau, \quad \mathcal{T}_r = \{t \in [0, \mathcal{T}_{sc}] : T_d(t) \cdot T_a(t) < 0\}.$$

The driving quality is evaluated using the well-known steering wheel reversal rate ( $SRR$ ), which is related to the steering wheel instability [34]. This metric is defined by counting the number of times that the steering wheel was reversed at a rate of at least 15 [deg/s]. Since  $SRR$  is directly related to visual distraction or high cognitive workload, an increased  $SRR$  could be interpreted in terms of increased risk.

b) *Subjective Evaluation:* Questionnaires were provided after each test to evaluate *subjectively* the driving performed with each strategy. There are four subjective factors: the driving control feeling (*Control*), the driving comfort (*Comfort*), the ease of obstacle avoidance (*Easiness*), and a subjective evaluation of the overall driving performance (*Performance*). The first three factors are reported over a scale of 0 (worst) to 100 (best). The last one is to simply check one of the three options: *Good*, *Medium* or *Bad*. A Student’s T-test for paired samples was used for statistical analysis of both objective and subjective data. The threshold of significance was set at 0.05.

## B. Experimental Results and Discussions

1) *Objective Results:* The objective results on driver-automation interaction obtained with each driving strategy are summarized in Fig. 10. The time consistency of the driver’s and the automation’s actions during the test with both **No-Shared** and **Shared** strategies is depicted in Fig. 10 (a). The T-test reveals a significant increase in time consistency under **Shared Control** compared to **No-Shared Control** with  $p$ -value = 0.03. The result in Fig. 10 (b) shows a clear increase in the effort consistency with **Shared Control**. The statistical test confirms this significant increase with  $p$ -value = 0.02. As presented in Fig. 10 (c), when the driving automation does not cooperate with the drivers under **No-Shared Control**, the effort required to steer the vehicle and to avoid the obstacles is very large compared to that obtained with **Manual Control** ( $p$ -value = 0.03). However, the T-test shows no significant difference between **Manual** and **Shared Control** strategies for the  $StE$  metric. It is also clearly observed in Fig. 10 (d) that using **Shared Control** strategy, the automation significantly reduces its resistance to the driver compared to **No-Shared Control** ( $p$ -value = 0.02).

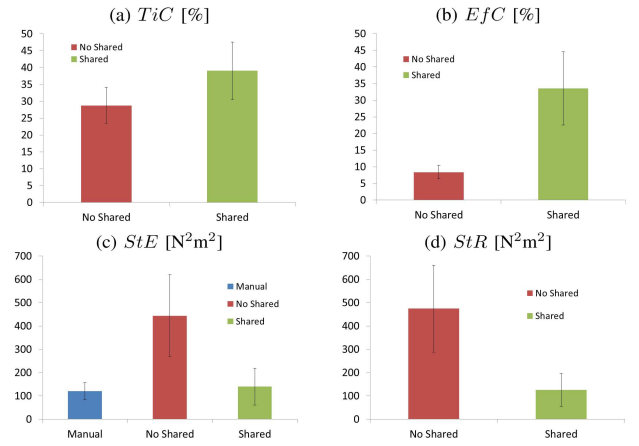


Fig. 10. Mean and standard deviation of: (a) Time consistency; (b) Effort consistency; (c) Steering effort; (d) Steering resistance.

The results on  $SRR$  obtained with different driving strategies are presented in Fig. 11. With both **No-Shared Control** and **Shared Control** strategies,  $SRR$  increases compared to that of **Manual Control** strategy. This means that the driving automation under both **No-Shared Control** and **Shared Control** strategies leads to a slight increase in the instability of the vehicle guidance compared to manual driving. In addition, the difference between these two strategies is not significant with respect to the  $SRR$  metric according to the T-test.

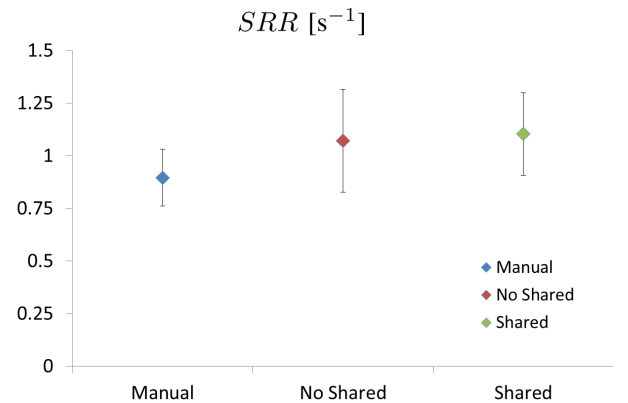


Fig. 11. Mean and standard deviation of  $SRR$  with three strategies.

The objective results demonstrate a clear improvement in terms of driver-automation interaction thanks to the proposed



trajectory planning algorithm used for **Shared Control**. This is due to the fact that the automation adaptively replans the vehicle trajectory according to the driver's actions, which results in an *active* driving assistance during obstacle avoidance. To emphasize the interests of the proposed trajectory planning, the results obtained with the first driver participant using three driving strategies are presented in Fig. 12 for illustrations.

As observed in Fig. 12 (b), with **No-Shared Control**, the assistive torque  $T_a$  is *constantly* opposite to the driver's torque  $T_d$ . This is explained by the fact that without using the cooperative planning algorithm, the driving automation only focuses on the lane keeping task when the driver performs obstacle avoidance maneuvers. Hence, the driver must provide a much larger  $T_d$  than  $T_a$  so that he could make necessary deviations to avoid the obstacles. This also results in a significantly higher  $T_d$  than that provided with **Manual Control** strategy, see Fig. 12 (a). Remark in Figs. 12 (a) and (c) that the driver's torque  $T_d$  required to perform the avoidance tasks with **Shared Control** is reduced and of the same order as with **Manual Control**. It can be also observed in Fig. 12 (c) that the planned trajectory  $y_p$  is *continuously* updated to better accommodate the driver's steering actions, which explains the above-mentioned increase in the driver-automation consistency when using **Shared Control** strategy. This is not the case of the results in Fig. 12 (b) with **No-Shared Control**, for which the planned trajectory  $y_p$  only corresponds to the lane centerline. However, during the test scenario there are phases where the planned trajectory  $y_p$  does not match that realized by the driver  $y_v$ , especially when the avoidance tasks must be quickly performed, see for instance the time interval [37s, 42s] in Fig. 12 (c). This is due to the parameterization of the proposed algorithm that favors trajectories minimizing the lateral acceleration for comfort reasons.

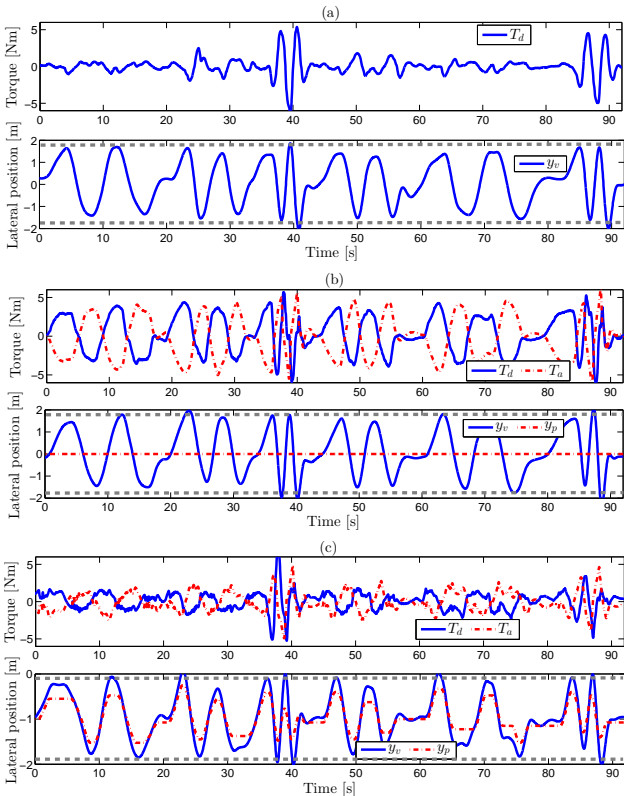


Fig. 12. Results obtained with the first driver participant. (a) **Manual Control**: Driver torque  $T_d$  and vehicle position  $y_v$ ; (b) **No-Shared Control**: Driver torque  $T_d$ , assistive torque  $T_a$  and vehicle position  $y_v$ , planned position  $y_p$ ; (c) **Shared Control**: Driver torque  $T_d$ , assistive torque  $T_a$  and vehicle position  $y_v$ , planned position  $y_p$ .

2) *Subjective Results*: The subjective results obtained with the considered test scenario are summarized in Fig. 13. Observe that the three subjective metrics *Control*, *Comfort* and

*Easiness* are lower with **No-Shared Control** strategy than to the two other ones. Also, the feeling of driving comfort and ease of obstacle avoidance is worse with **No-Shared Control** while **Shared Control** allows to have a driving feeling almost equivalent to that obtained with **Manual Control**. Moreover, the results on *Performance* metric shown in Fig. 13 (d) confirm that **No-Shared Control** strategy leads to the worst driving performance perceived during the test scenario. On the contrary, the subjective results show a clear improvement of the subjective feeling of drivers when using the proposed cooperative trajectory planning for **Shared Control** strategy. Indeed, a significant reduction of the steering wheel resistance and an *active* assistance that the driver has received during the obstacle avoidance maneuvers have contributed to increase the vehicle control feeling and the driving comfort in this case.

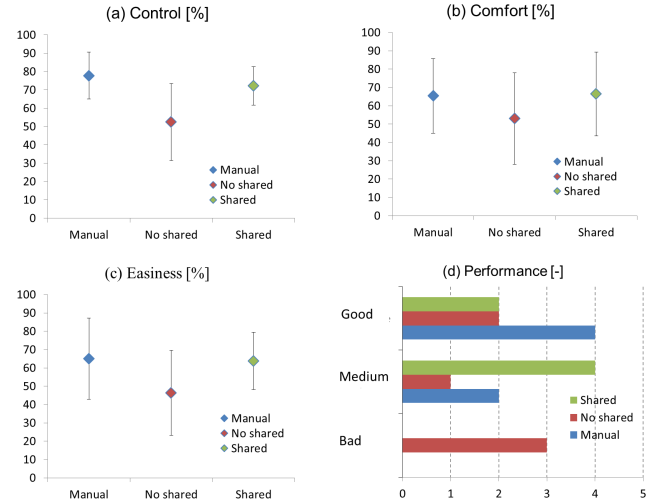


Fig. 13. Subjective results on the feeling of: (a) Driving control; (b) Driving comfort; (c) Ease of driving; (d) Overall driving performance.

## VI. CONCLUDING REMARKS

A novel cooperative trajectory planning algorithm is proposed for haptic shared driving control. In this study, the driver-automation conflict is characterized in the test scenario by the presence of *undetected* obstacles on the trajectory that must be performed by the automation. An *active* assistance can be achieved by adaptively updating the vehicle trajectory according to the driver's actions. This allows the driver to perform much more easily his/her desired trajectory, leading to a better feeling of vehicle control and driving comfort. The effectiveness of the proposed planning algorithm is clearly demonstrated with both objective and subjective evaluations. Future works focus on taking into account the obstacles in the cooperative planning algorithm to solve the driver-automation conflict. Moreover, as reported by participants during the post-experimental interviews, it would be interesting to integrate a visual feedback to display online the replanned trajectory. This could help drivers better understand the automation's actions to reduce further conflicts. Furthermore, user test experiments with an important number of driver participants will be required to study more thoroughly the *acceptability* of the proposed shared control method.

## REFERENCES

- [1] D. Abbink, M. Mulder, and E. Boer, "Haptic shared control: smoothly shifting control authority?" *Cogn. Technol. Work*, vol. 14, no. 1, pp. 19–28, Nov. 2012.
- [2] M. A. Benloucif, A.-T. Nguyen, C. Sentouh, and J.-C. Popieul, "A new scheme for haptic shared lateral control in highway driving using trajectory planning," *IFAC-PapersOnLine*, vol. 50, no. 1, pp. 13834–13840, Jul. 2017.

- [3] Z. Wang, R. Zheng, T. Kaizuka, K. Shimono, and K. Nakano, "The effect of a haptic guidance steering system on fatigue-related driver behavior," *IEEE Trans. Hum. Mach. Syst.*, vol. 47, no. 5, pp. 741–748, Oct. 2017.
- [4] M. Flad, L. Fröhlich, and S. Hohmann, "Cooperative shared control driver assistance systems based on motion primitives and differential games," *IEEE Trans. Hum. Mach. Syst.*, vol. 47, no. 5, pp. 711–722, Oct. 2017.
- [5] M. Li, H. Cao, X. Song, Y. Huang, J. Wang, and Z. Huang, "Shared control driver assistance system based on driving intention and situation assessment," *IEEE Trans. Indus. Inf.*, vol. 14, no. 11, pp. 4982–4994, Nov. 2018.
- [6] A.-T. Nguyen, C. Sentouh, and J.-C. Popieul, "Driver-automation cooperative approach for shared steering control under multiple system constraints: Design and experiments," *IEEE Trans. Ind. Electron.*, vol. 64, no. 5, pp. 3819–3830, May. 2017.
- [7] C. Sentouh, A.-T. Nguyen, M. Benloucif, and J.-C. Popieul, "Driver-automation cooperation oriented approach for shared lateral control design," *IEEE Trans. Control Syst. Technol.*, DOI 10.1109/TCST.2018.2842211, Jun. 2018.
- [8] K. Tanaka and H. O. Wang, *Fuzzy Control Systems Design and Analysis: A Linear Matrix Inequality Approach*. John Wiley & Sons, 2004.
- [9] D. González, J. Pérez, V. Milanés, and F. Nashashibi, "A review of motion planning techniques for automated vehicles," *IEEE Trans. Intell. Transp. Syst.*, vol. 17, no. 4, pp. 1135–1145, Apr. 2016.
- [10] B. Paden, M. Čáp, S. Z. Yong, D. Yershov, and E. Frazzoli, "A survey of motion planning and control techniques for self-driving urban vehicles," *IEEE Trans. Intell. Veh.*, vol. 1, no. 1, pp. 33–55, Mar. 2016.
- [11] E. Plaku, L. E. Kavraki, and M. Y. Vardi, "Motion planning with dynamics by a synergistic combination of layers of planning," *IEEE Trans. Rob.*, vol. 26, no. 3, pp. 469–482, Jun. 2010.
- [12] X. Li, Z. Sun, D. Cao, D. Liu, and H. He, "Development of a new integrated local trajectory planning and tracking control framework for autonomous ground vehicles," *Mech. Syst. Signal Process.*, vol. 87, pp. 118–137, Mar. 2017.
- [13] R. V. Cowlagi and P. Tsiotras, "Hierarchical motion planning with dynamical feasibility guarantees for mobile robotic vehicles," *IEEE Trans. Rob.*, vol. 28, no. 2, pp. 379–395, Apr. 2012.
- [14] S. Glaser, B. Vanholme, S. Mammari, D. Gruyer, and L. Nouveliere, "Maneuver-based trajectory planning for highly autonomous vehicles on real road with traffic and driver interaction," *IEEE Trans. Intell. Transp. Syst.*, vol. 11, no. 3, pp. 589–606, Sept. 2010.
- [15] T. Brandt, T. Sattel, and M. Bohm, "Combining haptic human-machine interaction with predictive path planning for lane-keeping and collision avoidance systems," in *IEEE Intell. Veh. Symp.*, pp. 582–587, Istanbul, Turkey, Jun. 2007.
- [16] M. Likhachev and D. Ferguson, "Planning long dynamically feasible maneuvers for autonomous vehicles," *Int. J. Rob. Res.*, vol. 28, no. 8, pp. 933–945, Jun. 2009.
- [17] D. Dolgov, S. Thrun, M. Montemerlo, and J. Diebel, "Path planning for autonomous vehicles in unknown semi-structured environments," *Int. J. Rob. Res.*, vol. 29, no. 5, pp. 485–501, Jan. 2010.
- [18] J. Nilsson, J. Silvén, M. Brannstrom, E. Coelingh, and J. Fredriksson, "If, when, and how to perform lane change maneuvers on highways," *IEEE Intell. Transp. Syst. Mag.*, vol. 8, no. 4, pp. 68–78, Winter 2016.
- [19] B. Gütjahr, L. Gröll, and M. Werling, "Lateral vehicle trajectory optimization using constrained linear time-varying MPC," *IEEE Trans. Intell. Transp. Syst.*, vol. 18, no. 6, pp. 1586–1595, Jun. 2017.
- [20] J. Chen, C. Liu, and M. Tomizuka, "FOAD: Fast optimization-based autonomous driving motion planner," in *Proc. Am. Control Conf. (ACC)*, pp. 4725–4732. Milwaukee, USA: IEEE, Jun. 2018.
- [21] J. Reeds and L. Shepp, "Optimal paths for a car that goes both forwards and backwards," *Pacific J. Math.*, vol. 145, no. 2, pp. 367–393, 1990.
- [22] C. Alia, T. Gilles, T. Reine, and C. Ali, "Local trajectory planning and tracking of autonomous vehicles, using clothoid tentacles method," in *Intell. Vehicles Symp. (IV)*, pp. 674–679. Seoul, South Korea: IEEE, Jul. 2015.
- [23] J. Funke, P. Theodosis, R. Hindiyeh, G. Stanek, K. Kritatakirana, C. Gerdes, D. Langer, M. Hernandez, B. Müller-Bessler, and B. Huhnke, "Up to the limits: Autonomous Audi TTS," in *Intell. Vehicles Symp. (IV)*, pp. 541–547. Alcalá de Henares, Spain: IEEE, Jul. 2012.
- [24] I. Papadimitriou and M. Tomizuka, "Fast lane changing computations using polynomials," in *Proc. Am. Control Conf. (ACC)*, vol. 1, pp. 48–53. Denver, USA: IEEE, Jun. 2003.
- [25] M. Werling, S. Kammel, J. Ziegler, and L. Gröll, "Optimal trajectories for time-critical street scenarios using discretized terminal manifolds," *Int. J. Rob. Res.*, vol. 31, no. 3, pp. 346–359, Dec. 2012.
- [26] J. Wei, J. M. Snider, T. Gu, J. M. Dolan, and B. Litkouhi, "A behavioral planning framework for autonomous driving," in *Proc. IEEE Intell. Vehicles Symp.*, pp. 458–464. Dearborn, USA: IEEE, Jul. 2014.
- [27] A. Doshi and M. M. Trivedi, "Tactical driver behavior prediction and intent inference: A review," in *14th Int. Conf. Intell. Transp. Syst. (ITSC)*, pp. 1892–1897. Washington, USA: IEEE, Nov. 2011.
- [28] D. Kasper, G. Weidl, T. Dang, G. Breuel, A. Tamke, A. Wedel, and W. Rosenstiel, "Object-oriented bayesian networks for detection of lane change maneuvers," *IEEE Intell. Transp. Syst. Mag.*, vol. 4, no. 3, pp. 19–31, Fall 2012.
- [29] A. Takahashi, T. Hongo, Y. Ninomiya, and G. Sugimoto, "Local path planning and motion control for AGV in positioning," in *Int. Workshop Intell. Rob. Syst.*, pp. 392–397. Tsukuba, Japan: IEEE/RSJ, Sept. 1989.
- [30] D. Koller, K. Daniilidis, and H.-H. Nagel, "Model-based object tracking in monocular image sequences of road traffic scenes," *Int. J. Comput. Vis.*, vol. 10, no. 3, pp. 257–281, Oct. 1993.
- [31] W. Hu, T. Tan, L. Wang, and S. Maybank, "A survey on visual surveillance of object motion and behaviors," *IEEE Trans. Syst., Man, Cybern., Part C*, vol. 34, no. 3, pp. 334–352, Aug. 2004.
- [32] R. Jazar, *Vehicle Dynamics: Theory and Application*. Springer-Verlag US, 2017.
- [33] A.-T. Nguyen, T. Laurain, R. Palhares, C. Sentouh, and J.-C. Popieul, "LMI-based control synthesis of constrained T-S systems subject to  $\mathcal{L}_2$  or  $\mathcal{L}_\infty$  disturbances," *Neurocomputing*, vol. 207, no. C, pp. 793–804, Sept. 2016.
- [34] W. A. Macdonald and E. R. Hoffmann, "Review of relationships between steering wheel reversal rate and driving task demand," *Human Factors*, vol. 22, no. 6, pp. 733–739, Dec. 1980.



**Amir Benloucif** received the M.Sc. degree in electronic systems and robotics from the University of Versailles, Versailles, France, in 2013, and the PhD degree in automatic control from the Université Polytechnique Hauts-de-France, Valenciennes, France, in 2018.

He is currently an engineer in automotive industry. His research interests include automotive control, cooperation in transportation systems.



**Anh-Tu Nguyen (M'18)** received the degree in engineering and the M.Sc. degree in automatic control from Grenoble Institute of Technology, Grenoble, France, in 2009, and the PhD degree in automatic control from the University of Valenciennes, Valenciennes, France, in 2013.

He is an Associate Professor at the Université Polytechnique Hauts-de-France, and a researcher at the laboratory LAMIH UMR CNRS 8201, Valenciennes, France. His research interests include robust control and observation, constrained systems, human-machine shared control with strong emphasis on vehicle engineering applications.



**Chouki Sentouh (M'17)** received the M.Sc. degree in automatic control from the University of Versailles, Versailles, France, in 2003, and the PhD degree in automatic control from the University of Evry, Evry, France, in 2007.

He was a postdoctoral researcher at the laboratory IRCCyN UMR CNRS 6597, France, from 2007 to 2009. Since 2009, he is an Associate Professor at the Université Polytechnique Hauts-de-France, laboratory LAMIH UMR CNRS 8201, France. His research fields include automotive control, driver

assistance systems with driver interaction, human driver modeling and cooperation in intelligent transportation systems.



**Jean-Christophe Popieul** received the PhD in automatic control from the University of Valenciennes, France, in 1994. He is a Professor of automatic control with the same university, laboratory LAMIH UMR CNRS 8201, Valenciennes, France. His research interests include transport safety, driver status assessment, shared control for full driving automation. Prof. Popieul is a member of several scientific boards, including ANR, PREDIT, i-Trans competitiveness cluster, IRT Railegium. He is also the Head of several Interactive Platforms of the LAMIH: the SHERPA driving simulator, the PSCHITT-Rail train/tramway simulator, and the PSCHITT-PMR wheelchair simulator.